



Review on the Acoustical Properties and Characterisation Methods of Sound Absorbing Porous Structures: A Focus on Microcellular Structures Made by a Replication Casting Method

A. J. Otaru¹

Received: 16 September 2019 / Accepted: 22 October 2019
© The Korean Institute of Metals and Materials 2019

Abstract

A comprehensive literature review on the acoustical properties and characterisation methods of sound-absorbing porous materials with a focus on the type made by a replication casting process (i.e. “bottleneck-type” structures as referred to in this work) is presented herein. The review describes in detail pore-structure related parameters of soundproofing devices; models used for predicting their acoustic absorption behaviour and techniques for enhancing their sound absorption potential. An extensive survey, that includes a presentation of the application of Wilson’s relaxation-matched equivalent fluid model to accurately predict the acoustic absorption spectra of “bottleneck-type” materials are given which could contribute to proposed research on the acoustic behaviour characterised by bimodal “bottleneck-type” structures.

Keywords Sound absorption · Porous structures · Review

1 Introduction

Sounds are part of our daily life experience, where sources of sound can be a vibrating speaker that sets the vibrating accord into motion, a running engine, pressure changes produced in a tsunami wave. The physical definition of sound is described as vibrations that propagate throughout a medium of air, or water, as a mechanical wave of pressure and displacement. The reception of such waves and perception by the brain is the physiological definition of sound [1]. Sound exists because of the interaction of the flow of fluid particles resulting in frictional contact and heat generation when they encounter a porous or solid body. As much as science deals with discovery, the acoustic engineer is encumbered with the responsibility of either enhancing sound or providing a solution for its reduction using sound-absorbing materials and equipment. Typical examples of sound-absorbing materials currently in use are glass wool fibres, hemp, kevlar, polyesters, wood, melamine, porous sintered fibre metals,

polyurethane [2–4] and more recently, artificially made porous metallic structures [5–11].

Porous metallic materials are categorised into open-celled and close-celled structures [12]. The close-celled metallic structures (Fig. 1a) are characterised by infinite airflow resistivity (ratio of fluid dynamic viscosity to permeability) and are generally termed as poor sound absorbers [5, 13]. The open-celled (Fig. 1b) metallic foam structures are composed of one or more solid phases and a gaseous phase. The gaseous phase allows fluid to flow or offers, or offers compressibility, while the solid phase provides geometrical architecture, strength, thermal conductivity, electrical conductivity, magnetic shielding and most importantly, its provision as an acoustic barrier [14–16]. In this case, viscous (windows) and thermal (pores) losses predominate sound energy-dissipation mechanisms when compared to the minimal contributions made by Helmholtz resonators, structural vibration and vortex shedding [17]. Though metal foams are quite expensive their ability to be recycled make them economically well-disposed of and would serve as an efficient absorber if it enhanced. A possible resolution is the utilisation of porous media models and structural variation during foam making processes [18].

Theoretical and experimental works in this area have shown the feasibility of using an aluminium foam structure with open and semi-open cells for acoustic absorption

✉ A. J. Otaru
otaru_12257@yahoo.com

¹ Department of Chemical Engineering, Federal University of Technology, P.M.B. 065, Minna, Nigeria

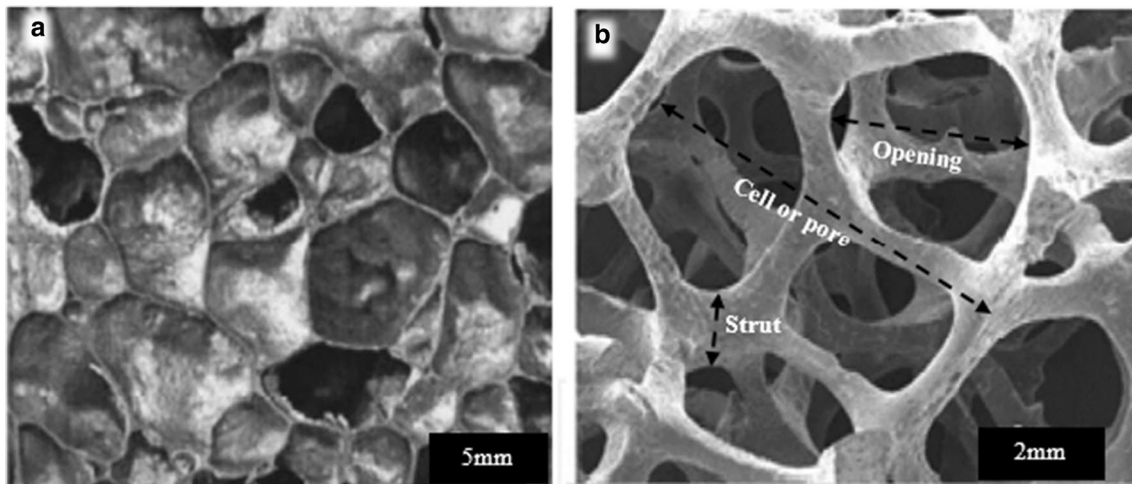


Fig. 1 Micrographs of **a** close-celled and **b** open-celled porous metallic structures. Sourced: from Ref. [12]

application. Lu and He [5] measured the static airflow resistivity and sound absorption coefficient for cellular metals with semi-open cells having different packing densities, pore sizes, and openings. Han et al. [19] showed that Al foam samples with a small nominal pore size (500 μm) exhibit the best absorption peak, when there is no air gap, and predominantly Helmholtz resonant absorption in the presence of an air gap. The influence of pore size, porosity and foam layer thickness on the acoustic performance of porous steel samples manufactured by a lost carbonate sintering process were further substantiated in [20]. Enhancing the sound absorptive performance of porous metallic structures was reportedly [17] carried out by hole-drilling or rolling techniques and insertion of appropriate air gaps [5, 7, 13] which predominantly becomes Helmholtz resonance absorption [19] with increased porous layer thickness [21, 22].

The unique and combined characteristics of low weight, high young modulus, low moisture absorption and excellent fire resistance of commercially available high-density porous metallic structures like RecematTM, PorvairTM and AlantumTM enable their suitability for high impact and load-bearing applications. However, numerically simulated hard-backed characteristic sound absorption spectra developed across these materials are relatively poor [10] when compared to the performance of hard-backed fibrous structures [3, 7], most specifically, in the region of their quarter wavelength hard-backed layer resonance frequencies (≤ 2.5 kHz). The sound absorption performance enhancement of these materials [10] was achieved by “structural-adaptation” of high-resolution tomography image data (dilation of the porous matrices) of the materials using 3D advanced imaging techniques in ScanIPTM. Such an approach resulted in reduced pore volume, pore size and pore openings of the materials thereby resulting in reduced permeability ($0.5\text{--}1.5 \times 10^{-09}$ m^2) of the materials for optimum acoustic

performance as shown in Fig. 2. Additionally, the sound absorption spectra of low-density, hard-backed “bottleneck-type” porous metallic structures characterised by monomodal spheres [9, 23] were observably poor for frequencies above 3.0 kHz. Alteration to the “bottleneck” structures to model more intricate monosized structures for pore sizes below 500 μm , and to explore the opportunity to which larger pore size structures could be functional, was done [23] to achieve optimum structural parameters required for the casting processes. The structure thrust back pressure wave to penetrate its interior cellular structure was achieved for pore diameter openings below 75 μm , but becomes a poor absorber for window diameter openings beyond 350 μm . The potential for the “bottleneck” structures to respond well to the absorption of sound pressure waves was achieved for permeabilities, porosities and window to pore ratio between $0.4\text{--}1.5 \times 10^{-09}$ m^2 , 60%–80% and 0.1–0.3 respectively (Fig. 3).

Applicable experimental and predictive studies reported in [3, 5, 6, 8, 24–29] have all described the characteristic sound absorption behaviour of porous materials as a function of structural properties and most importantly, the permeability of the porous medium. Research work [9, 11] showed reasonable correlation between measured and predicted characteristic sound absorption spectra for bottleneck structures using Wilson’s [28] relaxation-matched equivalent fluid models developed for predicting the sound-absorbing properties of structures characterised with circular pores and openings. Unlike the Johnson–Champoux–Allard (JCA) 5 parameters model, the Wilson model uses three pore-structure related parameters of the porous medium (permeability, porosity and tortuosity) to accurately describe the behaviour characterised by the boundary layer at the scale of the pores where there is a transition in the relaxation behaviour [11]. Knowing (or measuring) and predicting the pore-structure

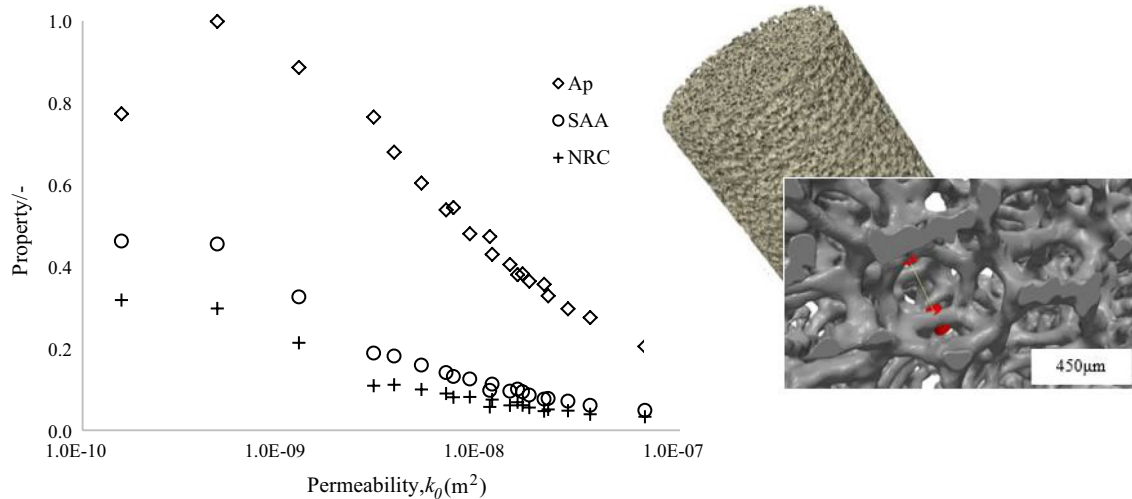


Fig. 2 Left of an optical and high-resolution tomography image data of an Incofoam (now Alantum) 450 μm , is plots of simulated maximum absorption peak (Ap), sound absorption average (SAA) and

noise reduction coefficient (NRC) against Darcian permeability (m^2) for the combined “real” and “structurally-dilated” metallic structures. Adapted from Ref. [10]

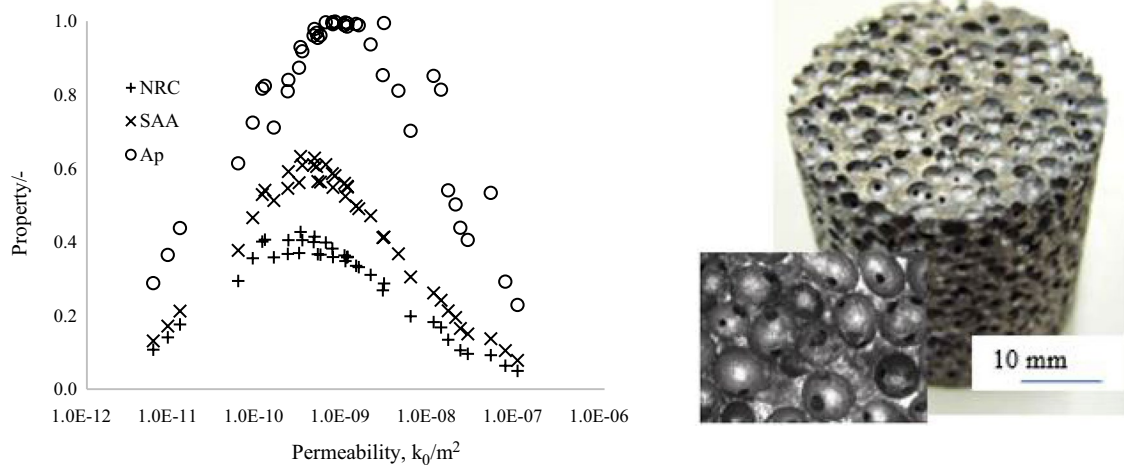


Fig. 3 Left of an optical and scanning electron microscopy image of a porous sample, is graphical representations of acoustic properties of numerically simulated “bottleneck-type” structures against permeability for pore sizes between 200 and 3000 μm . Adapted from Refs. [9, 23, 25]

related parameters of these ultralight and self-supporting structures (porous metals) is essential to the design and optimisation of enhanced materials (with novel attributes) capable of damping down vibration, such as in high-end loudspeakers (Fig. 4).

Modification and characterisation of the bottleneck structures [11, 23] were achieved using established equations [9] with assumed values for pore volume fractions ranging between 0.6 and 0.8%. Higher dip in the characteristic absorption spectra was reportedly observed for the low-porosity ($\epsilon \leq 0.7$) structures (See Fig. 5) and a progressive flattening in the sound absorption spectra (increasing

the sound absorption band) was observed with increasing pore volume fraction (ϵ) resulting in reduction of the high-frequency dynamic tortuosity (τ) of the materials. However, higher pore volume fractions (packing density) beyond 0.67 are difficult to achieve during the replication casting process for structures typified by near-spherical pores [5, 6, 30] except in cases where there is the presence of half-sized [29, 30] salt beads resulting in structural inhomogeneity of the porous metallic structures.

The use of virtual macroporous sphere-packing models developed [30] coupled with 3D advanced imaging techniques [21, 31–33] and computational fluid dynamics [25,

Fig. 4 Acoustical effects in loudspeaker design and to the right are the 25-ultimate audiophile speaker produced by Bowers and Wilkins (\$60,000/pair). Adapted from Ref. [23]

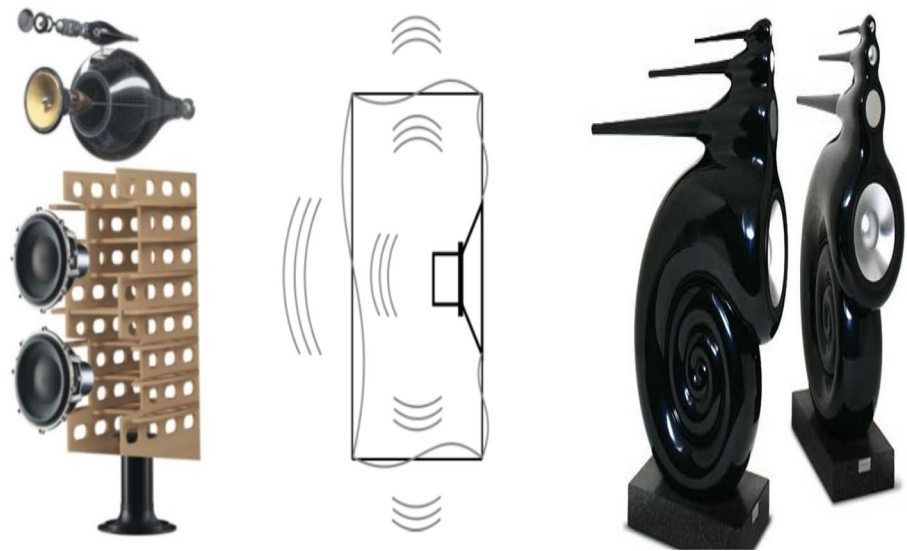
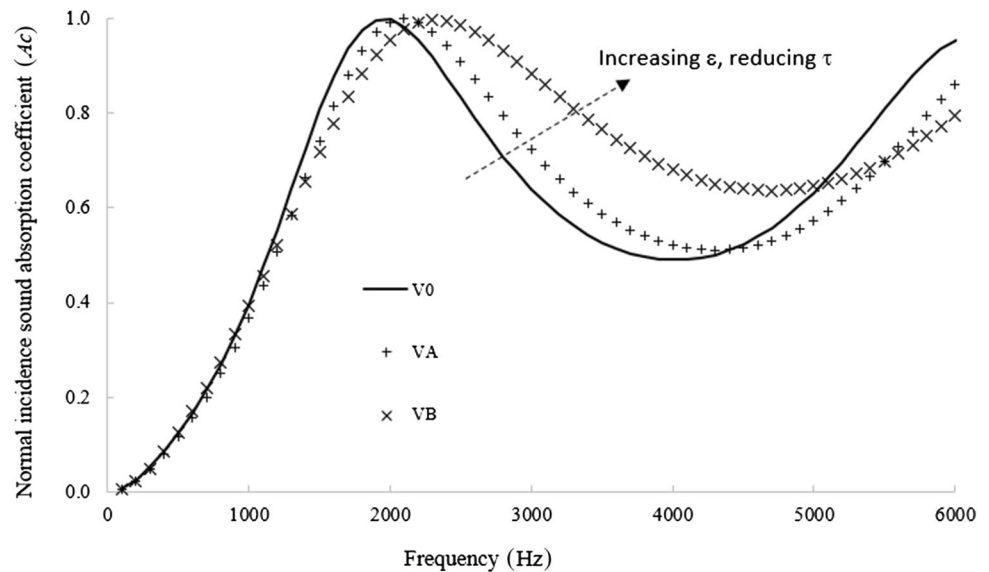


Fig. 5 Plots of simulated normal incidence absorption spectra (A_c) against frequency showing the effect of varying porosity (and tortuosity) at constant permeability. Adapted from Ref. [11]



[31] enables the quantitative assessment of pore-structure related parameters of the porous medium and may prove useful in predicting the characteristic sound absorption spectra of “bottleneck-type” structures. However, predictive and experimental data on the sound absorption spectra of replicated microcellular structures available in the literature [5, 6, 9, 25] most importantly, the “bottleneck-type” are limited to structures characterised by monomodal pores (similar pore sizes) with porosities ranging from loose (0.60) to densely packed (0.67) during casting. The sphere-packing models developed [30] showed that the porosity of the monomodal packings can be varied widely through the packing of spheres of different sizes which invariably result in changes in their pore-structure related parameters.

In light of these observations, a preliminary review on the acoustical properties and characterisation methods of

sound-absorbing porous materials with a focus on “bottleneck-type” macroporous structures is presented herein. This may serve as a basis for future work in experimental and numerical predictions of acoustical properties for both monomodal and bimodal “bottleneck-type” materials (using sphere-packing models) when subjected to the propagation of sound pressure waves at waffling frequencies.

1.1 Acoustic Absorption

The acoustic properties of sound-absorbing materials are often described by their absorption potential at over a range of frequencies. The absorption coefficient represents how much of the sound is absorbed. Sun et al., [34] described the sound absorption coefficient of a porous material as the ratio of sound intensity absorbed (I_a , W/m^2) to the incident sound intensity

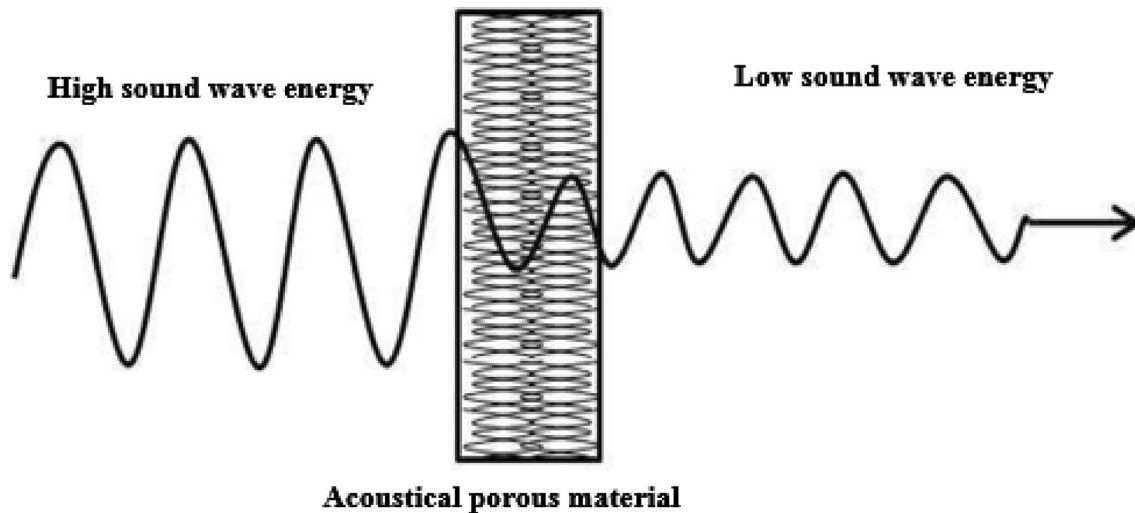


Fig. 6 Reducing high sound wave with an acoustic material. Adapted from Ref. [38]

(I_i , W/m²). Extensive work by Attenborough [35] and Umnova (2003) [34] expressed the derivation of a sound-absorption coefficient as a function of specific acoustic surface impedance (Z) and characteristic impedance (Z_c) of the porous material. This model has been validated by many researchers in the field of acoustics with nominal deviations between experimental and predicted values reported. Umnova et al. [36] reported that, when sound waves enter a pore or porous medium at an audible or higher frequency, sound energy is created, and a phase change occurs because of viscous drag and thermal exchange. More so, if this layer is backed by a rigid impervious wall on its rear face the analytical specific surface acoustic impedance reported in [37] was expressed as a function of sample thickness (L), sample porosity (ϵ), fluid density (ρ_o), propagation coefficient (k), fluid characteristic impedance (Z_c) and speed of sound in fluid (c_o) as shown by Eq. (2.1). The real (resistance) and imaginary (reactance) parts of this equation [3] are associated with energy loss and phase change of the acoustic field. Similarly, Wright [37] relates the sound absorption coefficient of a porous material as a function of their surface acoustic impedance, given in Eq. (2.1), and that of fluid (Z_o) as shown by Eq. (2.2).

$$Z = \frac{iZ_c \cot(kL)}{\epsilon \rho_o c_o} \quad (2.1)$$

$$A_c = 1 - \left(\frac{Z - Z_o}{Z + Z_o} \right)^2 \quad (2.2)$$

1.2 Techniques for Enhancing Acoustic Absorption

Elimination of resonance (vibration) and reduction of acoustical energy, to a certain extent, are considered in choosing

porous absorbing materials for us as soundproofing materials. The performance of acoustic materials is dependent on the amount of sound energy absorbed and represents the sound absorption characteristics [8] over a range of frequencies. Figure 6 represents the transmission of a high-pressure sound wave through a porous absorber to a low sound wave energy with the aid of an acoustical material [38].

The significance of metallic foam structures as an acoustic absorber in its ability to withstand microstructure manipulation, whilst conventionally available soundproofing fibrous materials such as wool, kevlar, melamine and polyurethane foam do not possess the strength to withstand mechanical alteration. The open-celled metallic structure allows propagated pressure waves to proliferate its network of smaller interconnected pores [19] and is considered beneficial in many application areas such as heat exchangers, sound absorbers, catalyst support system [39]. Close-celled foam structures (Fig. 1a) are generally considered poor sound absorbers owing to their propensity for greater reflection of sound waves from the metallic surface which can be reduced via rolling or cell fracturing [5, 40] to propagate to air movement. However, some of the cells' faces can break and become a passageway for sound pressure waves to fully penetrate the interior of the microstructure.

Extensive research has shown [41] that the sound absorption of porous materials are generally improved when the sound wave impacts smaller pores first. The size of the pores and connectivity of metal foams is one of its characteristic features leading to the defining characteristic absorption potential of the material. In the case of porous metals manufactured by a replication casting process (Fig. 3) of packed beds of salt beads, the structural morphology, pore size, pore openings and pore volume of the materials are not only defined by the filler size and shape but also in their packing density, arrangements

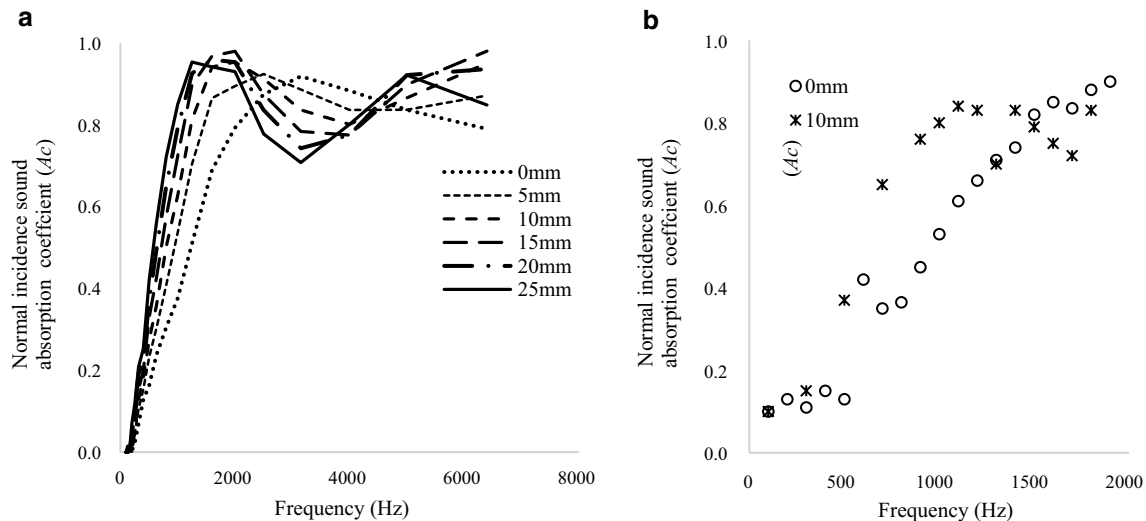


Fig. 7 Plots of measured sound absorption coefficient Frequency (Hz) for **a** polyurethane foam at airgap of 0, 5, 10, 15, 20 and 25 mm adapted from (adapted from Ref. [8]) and **b** hardbacked and 10 mm airgap “bottleneck-type” porous aluminium foam structure. Adapted from Ref. [5]

and the applied differential pressure used to drive the liquid melts into the convergent gaps created by the beads [23, 30, 31]. The interconnection of the fillers (touching spheres) determines the outcome of the resulting pore-structure related parameters of the porous materials. Other methods such as increased porous layer thickness, the presence of a back cavity or air gap, hole drilling/rolling of metal foams, and the patterns in the arrangement of the space fillers (packing of spheres) are considered in [6, 8, 23] for enhancing the sound absorption characteristics of porous metals.

The sound absorption coefficient of porous materials increases with an increase in sample thickness at different frequencies. Studies on combined polyethylene filled with metallic hydroxides and cross-linkable polyethylene [21] showed that the absorption peak of this material can be achieved even at low frequencies due to the extension of the pore channels resulting in significant fluid pressure drop and energy loss within the microstructure. The increasing pore non-uniformity in porous metallic structures (as a result of an increase in porous layer thickness) often results in an increase in their high-frequency dynamic tortuosity [42] and thereby shifting the quarter wavelength hard-backed layer resonance to lower frequencies. This was confirmed in experimental and computational work reported in [5, 6, 9–11, 22, 43, 44] for “bottleneck” dominated porous metallic structures with unique near-spherical pore diameter and apertures. An approximate relationship between the porous layer thickness, L , and selected frequency range, f , is numerically described in [22] in Eq. (2.3).

$$fL = \text{constant} \quad (2.3)$$

Experimental work on sound absorption measurements of polyurethane foams (Fig. 7a) [8], and porous

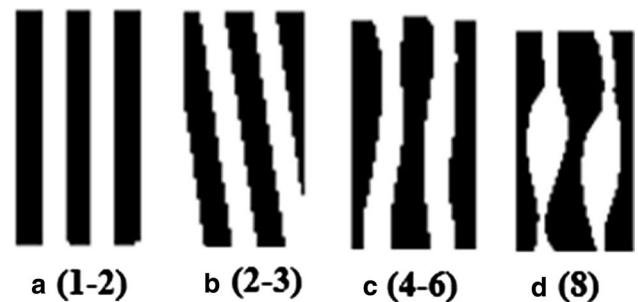


Fig. 8 Schematic representation of the growing complexity of motionless skeleton of **a** straight cylindrical pores **b** slanted cylindrical pores **c** non-uniform sections and **d** non-uniform sections with possible constrictions regarding the microstructure of the porous materials and the number of pore-structure related parameters needed to describe its sound absorption behaviour. Sourced: from <http://apmr.mateyls.com/index.html>

aluminium foams (Fig. 8b) [5] shows that an improvement in the characteristic absorption spectra of porous structures is observed with the insertion of a back cavity or airgap, resulting in a shift in the characteristic absorption frequency minima as compared to hard-backed measurements. The air medium provides additional resistance to the unabsorbed transmitted wave from the material where the soundwave becomes weak due to friction with air particles converting sound energy into heat. The mechanism for sound wave dissipation in air is described [43, 45, 46] as the Helmholtz resonance effect. Reducing the thickness of an acoustical material while maintaining its absorption potential can also be done by inserting an airgap.

1.3 Pore-Structure Related Parameters

The pore-structure related parameters used to describe the vibroacoustic behaviour of porous materials are classified into two categories: structural and elastic parameters. The pore-structure related parameters are associated with the interaction between a fluid and solid phases in the material. The number of parameters used in models to predict acoustical behaviour can vary between 1 and 8 depending on the material under consideration and associated structural morphology. Figure 8 shows the growing complexity of a motionless skeleton frame and appropriate models developed to represent the acoustic behaviour of these microstructures. These pore-structure related parameters of the are: open porosity (ϵ), high-frequency limit of the dynamic tortuosity (τ) and the airflow resistivity, (σ), which can be directly measured, while viscous characteristic length, (Λ), thermal characteristics length, ($\bar{\Lambda}$), static thermal permeability (k'_0), static viscous (τ_0) and static thermal (τ'_0) tortuosity are estimated from characterisation techniques (Acoustic Porous Material Recipes, APMR). Though the last three parameters are rarely used as they still need further development with respect to experimental characterisation [47]. Analytical models proposed in [48] could prove useful in the determination of these three pore-structure related parameters of porous matrices. The elastical parameters describe the viscoelastic behaviour of the solid phase of the material. Studies of acoustical porous media are usually limited to small deformation vibrations parameters reduced to 'elastical and damping' (Young's moduli, Poisson's ratio and structural damping coefficients).

1.3.1 Static Airflow Resistivity

The static airflow resistivity (σ) commonly referred to as resistivity and porosity (ϵ) are the two most well-known pore-structure related parameters, used to describe the acoustical behaviour of porous materials. The resistivity of a porous material is defined as the ratio of static gas pressure to airflow speed. It reflects the air permeability through porous materials and is also defined as the resistance within a unit thickness of material [21]. A mathematical expression for the relationship between static airflow resistivity and permeability (k_o) or pressure drop across a unit length (∇p) is given by Eq. (2.4). Some authors prefer to use static viscous permeability (k_o) which has the dimensions of a surface (m^2) with unit N s m^{-4} . The term μ is the dynamic viscosity of air ($\sim 1.80 \times 10^{-5} \text{ N s m}^{-2}$) at ambient temperature and pressure whilst v is the fluid velocity and L is the thickness of the porous body. The major difference between k_o and σ is that the former does not depend on the fluid property while the latter is specific to a fluid [49]. Equation (2.4) indicates that a high airflow resistivity is an indication of the low

permeability of the material. Such a porous material will require high pressure for fluid to constrict through [50]. In other words, if a fluid passes through a porous structure easily, such material has high permeability, low airflow resistivity and requires low pressure to compress the fluid. This airflow resistivity can also be measured using a flowmeter and permeability of a material and is often measured in m^2 .

$$\sigma = \mu/k_o \quad \text{or} \quad = \frac{\Delta P}{vL} \quad (2.4)$$

1.3.2 Open Porosity

Unlike the permeability (k_o) of a porous structure, defined as a measure of the flow resistance through the porous body, the open porosity (ϵ) commonly reduced to porosity, refers to the ratio of the fluid volume occupied by a continuous fluid phase to the total volume of a porous body [51]. It is also defined as the ratio of interconnected pore fluid volume (v_f) to the total bulk volume (V_B) of a porous aggregate [47, 52]. Kennedy [18] reported that porosity and pore size of replicated the "bottleneck" dominated structures can be controlled through the variation of space holder (salt beads) sizes and packing densities used during the manufacturing process. Dullien [52] also showed that the displacement method for the bulk volume and fluid saturation method for the pore volume can be used to measure the porosity of porous materials. Similarly, the porosity of porous metallic structures can also be measured with the aid of a porosimeter. This method is called mercury intrusion porosimetry and it provides reliable information about the pore size, specific surface, pore-volume, density and particle distribution of the microstructure [50, 53, 54]. High-resolution tomography images of "real" porous materials [55–58] combined with 3D advanced image processing routes involving volume rendering, segmentation, 3D editing, thresholding filtering [10, 23, 25, 31–33] also enables a quantitative assessment of the pore volume fraction (and other pore-structure related parameters) of porous metallic materials.

1.3.3 High-Frequency Limit of Dynamic Tortuosity

The high-frequency limit of dynamic tortuosity often reduced to tortuosity [59] is a property of a curve being tortuous (twisted; having many turns). For porous structures, tortuosity is defined as interconnectedness or sinuosity of the pore space [60] or the ratio of the shortest path to boundary distance for a porous structure. It can also be defined as a measure of how convoluted a path a fluid element travels between two points within a medium [48].

The equation describing the tortuosity of porous media flow can be traced back to Archie [61] and Winsauer et al. [62]. Archie [61] inferred the equation for the tortuosity

from experimental data as given in Eq. (2.5) while Winsauer et al. [62] measured tortuosity by an independent electrical method (Eq. 2.6).

$$F_r = af^{-m} \quad (2.5)$$

$$\tau^{1.67} = \varepsilon F \quad (2.6)$$

where a is a constant value close to 1.0; F_r is the formation resistivity; ε is the fractional porosity where $1.4 < m < 2.3$ exist for unconsolidated sands to indurated sandstone and 1.0 for straight pore. Occasionally crude approximations are generally used when tortuosity serves as the basis for predictions. For example, it is common practice to make tortuosity the inverse of porosity in the case of molecular diffusion [63]. For a straight path, tortuosity is 1.0; for porous metallic structures it is between 1.00 and 3.00 and for a circle, it is infinite [47]. The Johnson et al. [59] semi-phenomenological model uses the high-frequency limit of the real part of dynamic tortuosity to account for the visco-inertial interaction of the fluid in pores with a skeleton frame. This interaction makes the effective fluid heavier than the pore filled fluid [64, 65]. This is the main reason the defined tortuosity is always greater than unity. In a separate study, tortuosity was accounted for by using theoretical (Eq. 2.7) studies on diffusivity transport in porous systems consisting of spontaneously overlaying monosized spheres [66, 67]. Johnson et al. [59] proposed the high-frequency limit of dynamic tortuosity as a function of the material homogenization volume V , and fluid particle velocity (v) at high frequencies Eq. (2.8).

$$\tau = 1 - 0.25 \ln(\varepsilon) \quad (2.7)$$

$$\tau = \frac{\frac{1}{v} \int_V v^2 dV}{\left(\frac{1}{v} \int_V \vec{v} dV\right)^2} \quad (2.8)$$

Bhattacharya et al. [67] proposed the tortuosity of aluminium foam structures as functional geometrical value, G (0.5831 and 1.00) for porosity of 97% and 85%, respectively, with G interpolated with the given range of porosity (Eq. 2.9). They also considered that their model was valid for predicting pressure drops (Eq. 2.10) over a wide range of porosities in porous metallic structures.

$$\frac{1}{\tau} = \frac{\pi}{4\varepsilon} \left[1 - \left(\frac{1.18}{G} \sqrt{\frac{1-\varepsilon}{3\pi}} \right)^2 \right] \quad (2.9)$$

$$\frac{\Delta p}{LV} = \frac{\mu(1-\varepsilon)^2}{\varepsilon^3} \cdot \frac{\tau^2 \sigma}{\tau - 1} + \frac{(1-\varepsilon)}{\varepsilon^3} \cdot \frac{\tau^2 \sigma}{6} \cdot \rho V \quad (2.10)$$

Du Plessis et al. [68] gives a mathematical expression of the tortuosity for high-porosity porous metallic structures as a function of open porosity (Eq. 2.11) which was further rationalised by Du Plessis and Fourie [69] as shown by Eq. (2.12). Their expression was based on geometrical modelling of the internal structure of the porous material for a much smaller viscous boundary layer compared to the characteristic size of the pores of porous structures.

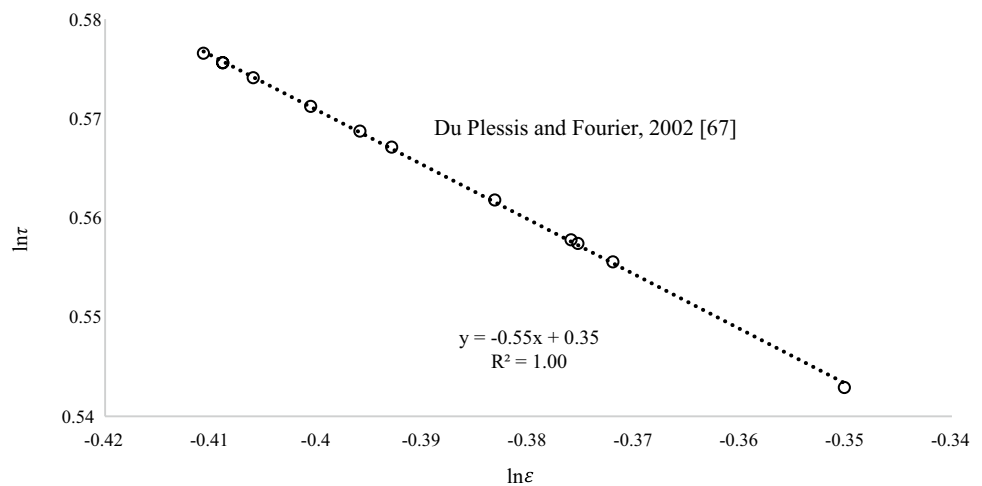
$$\frac{1}{\tau} = \frac{3}{4\varepsilon} + \frac{\sqrt{9-8\varepsilon}}{2\varepsilon} \cos \left\{ \frac{4\pi}{3} + \frac{1}{3} \cos^{-1} \left[\frac{8\varepsilon^2 - 36\varepsilon + 27}{(9-8\varepsilon)^{3/2}} \right] \right\} \quad (2.10)$$

$$\tau = 2 + 2 \cos \left[\frac{4\pi}{3} + \frac{1}{3} \cos^{-1}(2\varepsilon - 1) \right] \quad (2.11)$$

where ε and τ are the porosity and high-frequency limit of dynamic tortuosity of the porous body.

To establish confidence in the applicability of the tortuosity model developed in [69] (Eq. 2.11) and its suitability to accurately predict the dynamic tortuosity of “bottleneck-type” structures, a reliability test was carried out using the porosities (pore volume fractions) of virtual macroporous monosized structures characterised by having pore sizes between 1 and 3 mm and capillary radius between 10 and 80 μm , as reported in [25]. For an isotropic porous material with a random distribution of solid particles and voids, Dias et al. [70] proposed an exponential model ($\tau = C_o \varepsilon^{-n}$) relating the high-frequency limit of the dynamic tortuosity (τ) as a function of sample pore volume fraction (ε), shape factor, (C_o) and tortuosity factor (n). This tortuosity factor (n) is in fact known as the Bruggeman’s relationship and is related to the grain shape of a porous material, being 0.5 for spheres and between 0.4 and 0.6 for most porous metallic structures [70]. A plot of natural log of the high-frequency limit of dynamic tortuosity against the natural log of pore volume fraction computed for the “virtually-derived” porous structure for pore sizes ranging between 1 and 3 mm, pore volume fractions between 0.67 and 0.69, and capillary radius between 10 and 80 μm [25], shows a linear inverse relationship where a coefficient of determination ($R^2 \sim 99.9\%$) and tortuosity factor, $n \sim 0.55$ (Fig. 9) were attained. This theoretical model yielded explicit expressions indicating reliable predicted values of high-frequency limits of dynamic tortuosity which lies within the lower and upper bound tortuosity factor of 0.4 and 0.6 respectively, given for most porous sound-absorbing materials [71] and close to the 0.5 value predicted for spheres. Predicted data using this model is thought to be in good agreement with experimental data [70] and is well documented in [71]. The applicability of this tortuosity model to predict the dynamic tortuosity of bimodal structures (bimodal pores) has not yet been reported in the available literature and may form an integral part of proposed future

Fig. 9 Graphical representation of natural log of the high-frequency limit of tortuosity ($\ln\tau$) against natural log of pore volume fraction (porosity, ϵ) using analytically predicted values reported in Ref. [70] (Tortuosity factor, n is 0.552, shape factor, C_o is 0.35 with a very good fit $R^2 = 1.00$)



work on the acoustical properties of bimodal “bottleneck structures.

1.3.4 Viscous and Thermal Characteristic Lengths

One of the main advantages of pore-level numerical simulation over macroscale simulation is the enhancement of pore geometry and a localised view of the porous structure. This enables a good understanding of the internal structure (cell size, openings, surface area and tortuosity) of the porous medium in relation to its hydrodynamic or pressure wave behaviour. This porous structure consists of a connected metal frame (skeletal phase) saturated with air (occupying the porous region). When sound pressure waves propagate the pores and openings of a porous structure at an audible frequency, elevated sound energy is created resulting in the formation of viscous and thermal layers. Thus, the dissipation of acoustical energy through a porous material involves visco-inertial, thermal and structural dissipation effects [47].

The dissipation resulting from the friction of air particles within the structural walls as sounds propagating through the porous material is termed the viscous-inertial dissipation effect. A thermal wave is created as a result of successive compression and dilatation when sound waves propagate through the porous medium. The thermal dissipation effects exist when there is significant heat exchange between air particles and structural walls. The heat exchanged between the particles of air and structural frame results in the creation of a thermal boundary layer [72]. This definition justifies that both the viscous and thermal characteristic lengths are classified as pore-structure related parameters as it depends on the fluid and the localised pore geometry of the porous sample. The structural dissipation is dependent on the mechanical properties of the material. Although the nature of the skeletal frame of porous metals is largely dependent on the processing route employed, it can be changed by mechanical compression and rolling techniques as detailed earlier. Figure 10 presents a diagrammatic

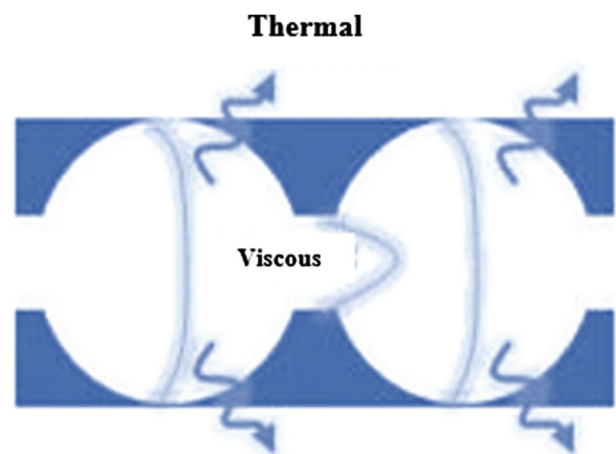


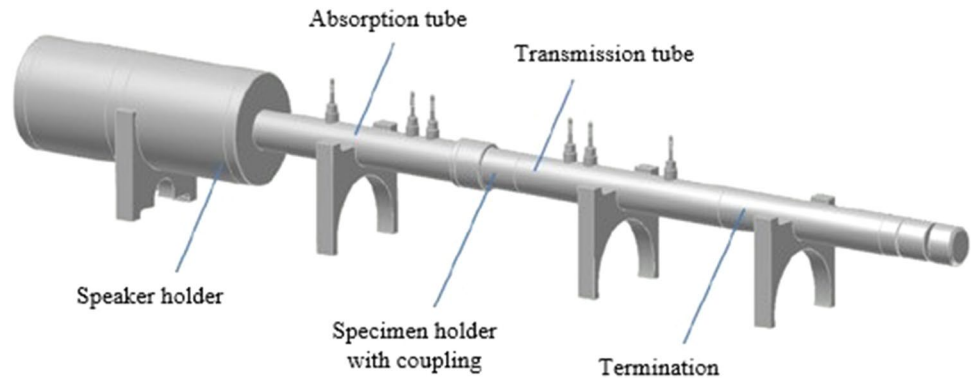
Fig. 10 Schematic view of viscous and thermal characteristics lengths. Adapted from Ref. [73]

representation of the viscous (window or pore diameter openings) and thermal (pore diameter size) characteristics length of porous material (adapted from [73]).

The application of the Johnson et al. [24, 27, 59] semi-phenomenological model to predict the acoustical behaviour of porous materials requires characterisation of the viscous and thermal characteristic lengths using scanning electron microscopy, optical imaging or X-ray computerised tomography techniques. Johnson et al. [59] expresses the viscous characteristic length (Λ) to be twice the ratio of the weighted by the velocity in the volume to that of the surface of an inviscid (low or no viscosity) fluid (Eq. 2.12) whilst the thermal characteristic length ($\bar{\Lambda}$) is a generalisation of a hydraulic radius and is defined as equal to twice the interconnected pore volume to pore wet surface ratio (Eq. 2.13).

$$\Lambda = 2 \frac{\int_{\Omega} v^2 dV}{\int_{\partial\Omega} v^2 dS} \quad (2.12)$$

Fig. 11 A 4-microphone, AFD 1200-AcoustiTube[®] measuring setup with sample holding section used to estimate the tortuosity, static thermal permeability, viscous and thermal characteristics length of porous structures



$$\bar{\lambda} = 2 \frac{\int_{\Omega} dv}{\int_{\partial\Omega} dS} = 2\Omega_f / \partial\Omega \quad (2.13)$$

where v is the superficial fluid local velocity, Ω_f is the inter-connected pore fluid volume, Ω is the bulk volume of the porous aggregate (computational domain), $\partial\Omega$ is the pore wet surface ratio (or fluid–solid or domain boundary), V and S are classified as volume and surface area.

The average radius of the smaller pores (pore windows) was described in Ref. [59, 73] to be the viscous characteristic length while that of the larger pores (pore sizes) to be the thermal characteristic length. A mathematical relation of viscous characteristic length for most porous materials without noticeable pore roughness and that of slit-like pores were also proposed in Johnson et al. [59] to be a function of the low-frequency limit of dynamic tortuosity ($\tau = 1/\cos^2 \theta$), permeability (k_o) and porosity (ϵ) of the porous structure as presented in Eqs. (2.14) and (2.15) respectively. They also specified the range of viscous characteristic length values between 11 and 350 μm as optimum for enhanced sound absorbing materials characterised by a network of “polyurethane-like” structures.

$$\Lambda = \sqrt{\frac{8\tau k_o}{\epsilon}} \quad (2.14)$$

$$\Lambda = \sqrt{\frac{12\tau k_o}{\epsilon}} \quad (2.15)$$

With known values of pore size, connectivity, permeability, porosity, and high-frequency limit of dynamic tortuosity, modelling of the characteristic acoustic impedance and sound absorption spectra of porous metallic structures using well-known equivalent fluid models for rigid-porous materials such as Attenborough, Delany–Bazley–Miki (DBM), Johnson–Champoux–Allard (JCA), and Wilson relaxation-matched models is possible. The application of the Johnson–Champoux–Allard–Lafarge (JCAL) and Johnson–Champoux–Allard–Prides–Lafarge (JCPL) models require determination of the remaining three parameters,

typically static thermal permeability (k'_o), static viscous tortuosity (τ_o) and static thermal tortuosity (τ'_o), using dimensionless shape factors (See Eq. 2.16) defined in [50]. Considerable work reported in [24] highlighted that the dimensionless shape factor defined by Eq. 2.16, M'_1 , equals unity (1.0) for structures with identical circular pores, 0.66 for slit, 0.3 for foam and 0.03 for glass wool. Using measured pore structure-related parameters of “bottleneck-type” aluminium structures [6], computed values of this shape factor (M'_1) were close to unity and in a similar trend, other dimensionless shape factors (M_1, N_1 and N'_1) are also equal to unity, but may differ from M'_1 depending on the pore morphology.

$$M_1 = \frac{8\tau}{\epsilon\bar{\lambda}^2} k_o \quad M'_1 = \frac{8}{\epsilon\bar{\lambda}^2} k'_o \quad N_1 = \frac{M_1}{4(\tau_o/\tau - 1)} \quad N'_1 = \frac{M'_1}{4(\tau'_o - 1)} \quad (2.16)$$

Acoustic engineers have worked out different methodologies for measuring pore-structure related parameters of porous structures using acoustical and non-acoustical methods. The main non-acoustical approach is used for characterising airflow resistivity and tortuosity [74]. The acoustical method is subdivided into low and high-frequency methods. The low-frequency method is based on using an impedance tube while the high-frequency method is based on ultrasonic techniques [75]. For a complete characterisation of the tortuosity, static thermal permeability, viscous and thermal characteristic lengths simultaneously, Zielinski [64] suggested inverse identification methods using a standing wave tube (as shown by Fig. 11) to account for the characteristic sound absorption spectra of porous structures. Thus, measurement of the sound absorption coefficient of porous metallic structures can be carried out in an AFD 1000-AcoustiTube[®] 2- or 4-microphone impedance tube in accordance with Analysis Software AFD 1001 user guide whose working principle is based on ISO 10534-2:2001 transfer-matrix method credited to Song and Bolton [76] and used by Han et al. [19] for acoustic absorption determination of porous Al foams. This allows the direct computation of the normal incidence sound absorption coefficient,

reflection coefficient and the surface acoustic impedance of porous absorbers according to the ISO standard. The standing wave tube method has the advantage of small sample requirements (40 mm maximum thickness) and is generally reproducible when compared to the reverberation time method [19]. Chu [77] and Han et al. [19] suggested that the transfer function approach, which uses the broadband random signal as a sound source, measures the impedance ratio of test materials and their normal incidence absorption or reflection coefficient at a much faster rate with good results and low at cost.

1.4 Acoustic Porous Media Models

The propagation of sound waves in an isotropic homogeneous material is determined by complex quantities the characteristic impedance (Z_c), and the propagation coefficient (k), [78]. The propagation coefficient is sometimes called the complex wave number, and is given by Eq. (2.16),

$$Z_c = R + iX = \sqrt{\rho_{(w)}K_{(w)}} \quad \text{and} \quad k = A + i\beta = w\sqrt{\frac{\rho_{(w)}}{K_{(w)}}} \quad (2.16)$$

where $K_{(w)}$ is the bulk modulus, $\rho_{(w)}$ is the effective density, w is the angular/radial or circular frequency mathematically described as $2\mu f$, R is termed the complex acoustic resistance, X is the complex acoustic acceptance, A is the attenuation constant (nepers/m; 1 neper is 8.68 dB) and β is the phase constant (rad/m).

The propagation of sound pressure waves in porous media can be described by propagation models. These propagation models are classified as either “equivalent solid” (uniform pressure), “equivalent fluid” (motionless skeleton) and/or the Diphasic (Biot’s theory) models (Acoustic Porous Material Recipes, APMR). For a given frequency range and appropriate boundary conditions, the skeletal frame (equivalent fluid) or fluid (equivalent solid) is considered motionless with no pressure wave propagating through the solid (equivalent fluid) or fluid (equivalent solid) phase of the microstructure. When waves propagate in both phases, it is termed Diphasic and described by Biot’s theory. Biot theory is most reliable in describing the vibroacoustic of porous materials [79]. Several models have been developed considering the contributions of skeletal and fluid phases over a certain frequency range. Typical examples are Zwikker and Kosten [80], Biot [79], Attenborough [35], Delany and Bazley [78], Miki [26], Allard and Champoux [81], Johnson et al. [59], Wilson [28] and William [82] models.

1.4.1 Primeval Models

Extensive research at the Technische Hogeschool in Delft city, Netherlands provided a cardinal and practical model describing the acoustic behaviour of porous materials with elastic frames [80]. The proposed Zwikker–Kosten [80] models depicted the static air pressure (P_o) and force acting on the skeletal frame per unit cross-section (P_m) as a function of the mean velocity of solid material (v_m) and that of air (v_o), density of the skeletal (frame) material (ρ_m) and that of air (ρ_o), open porosity of the porous material (ϵ), incompressibility modulus of air (K_o), specific frame thickness (L_m) and coupling coefficient (S) defined in terms of angular frequency in (Eqs. 2.17–2.21).

$$-\frac{\partial P_m}{\partial x} = \rho_m \frac{\partial v_o}{\partial t} + S(v_o - v_m) \quad (2.17)$$

$$-\frac{\partial P_o}{\partial x} = \rho_o \frac{\partial v_m}{\partial t} + S(v_m - v_o) \quad (2.18)$$

$$-\frac{\partial P_m}{\partial x} = L_m \frac{\partial v_o}{\partial x} - \frac{(1 - \epsilon)}{\epsilon} \frac{\partial P_o}{\partial t} \quad (2.19)$$

$$-\frac{\partial P_o}{\partial x} = \epsilon K_o \frac{\partial v_m}{\partial x} - (1 - \epsilon)(K_o - P_o) \frac{\partial v_o}{\partial t} \quad (2.20)$$

$$S = jw\rho_o(\tau - 1) + \epsilon^2 \quad (2.21)$$

The stated differential equations have been used for the study of elastic porous materials and were further expatiated by Biot [79] by improving the coupling coefficient for a better approximation of the structural frame and understanding of the fluid–structure interactions when pressures waves penetrate the interior cellular structure of a porous material. Keith Attenborough [83] modified the Zwikker–Kosten equations to predict the acoustical characteristics of sand and rigid fibrous absorbent soil as a function of five structural parameters namely: open porosity (ϵ), tortuosity (τ), steady shape factor (C_o), dynamic shape factor (C_D) and flow resistivity (σ). The model was developed to give accurate predictions of the characteristic absorption behaviour of a porous structure with improved statistical fit to measured data.

Working from a series of experimental data in fibrous materials with porosities close to unity, Delany and Bazley [78] proposed empirical expressions for the characteristic acoustic impedance (Z_c) and complex wavenumber (k) using the +jw t (sinusoidal time variation) time convention (Eqs. 2.22, 2.23). The validity of this expression was observed in [78] to be between $0.01 < \frac{f}{\sigma} < 1.00$. That is, suitable for very low frequencies (< 100 Hz) but not for very high frequencies (> 10 kHz) for fibrous materials [84]. Only one parameter (typically, the static airflow resistivity, σ) was needed to describe the acoustic behaviour of porous materials

using this model. Allard and Champoux [81] employed experimental data in [78] using the same range of frequencies and presented an expression for the characteristic acoustic impedance (Z_c) (Eq. 2.24) and propagation coefficient (k) (Eq. 2.25) with a close agreement between the two models.

$$Z_c = \rho_o C_o \left[1 + 9.08 \left(10^3 \frac{f}{\sigma} \right)^{-0.75} - j11.9 \left(10^3 \frac{f}{\sigma} \right)^{-0.73} \right] \quad (2.22)$$

$$k = \frac{w}{C_o} \left[1 + 10.8 \left(10^3 \frac{f}{\sigma} \right)^{-0.70} - j10.3 \left(10^3 \frac{f}{\sigma} \right)^{-0.50} \right] \quad (2.23)$$

$$Z_c = \rho_o C_o \left[1 + 0.0571 \left(\rho_o \frac{f}{\sigma} \right)^{-0.754} - j0.0870 \left(\rho_o \frac{f}{\sigma} \right)^{-0.732} \right] \quad (2.24)$$

$$k = \frac{w}{C_o} \left[1 + 0.0978 \left(\rho_o \frac{f}{\sigma} \right)^{-0.70} - j0.1890 \left(\rho_o \frac{f}{\sigma} \right)^{-0.50} \right] \quad (2.25)$$

For the case of multiple layers, Miki [26] observed that the real part of the surface impedance, when computed with the Delany and Bazley [78] model, sometimes became negative at low frequencies. From the same experimental data by Delany and Bazley [78], Miki proposed modifications of these expressions to amend the characteristic acoustic impedance (Z_c) and propagation coefficient (k) which was termed the Delany–Bazely–Mikki models as shown by Eqs. (2.26) and (2.27) respectively. Though, Miki takes care not to extrapolate the boundaries ($0.01 < \frac{f}{\sigma} < 1.00$) even when he had observed his revised expressions are well characterised for a larger frequency range, in particular $\frac{f}{\sigma} < 0.01$, $0 < \varepsilon < 1.0$ and $1000 < \sigma < 50,000$ Pa s/m².

$$Z_c = \rho_o C_o \left[1 + 5.50 \left(10^3 \frac{f}{\sigma} \right)^{-0.632} - j8.43 \left(10^3 \frac{f}{\sigma} \right)^{-0.632} \right] \quad (2.26)$$

$$k = \frac{w}{C_o} \left[1 + 7.81 \left(10^3 \frac{f}{\sigma} \right)^{-0.618} - j11.43 \left(10^3 \frac{f}{\sigma} \right)^{-0.618} \right] \quad (2.27)$$

1.4.2 Visco-Inertial and Thermal Effects Using Johnson et al. Acoustic Models

To accurately model acoustics for geometries with small dimensions, it is necessary to include thermal conduction effects and viscous losses explicitly in the governing equations. Having studied the acoustic behaviour of porous materials with a motionless skeleton frame having arbitrary pore

shapes, Johnson et al. [59] proposed a semi-phenomenological model to describe its complex density (Eq. 2.28). Four parameters are involved in the calculation of the dynamic density, open porosity (ε), static airflow resistivity (σ), the high-frequency limit of the tortuosity (τ), and the viscous characteristic length (Λ).

$$\rho_{(w)} = \tau \frac{\rho_o}{\varepsilon} \left\{ 1 + \frac{\sigma \varepsilon}{i w \rho_o \tau} \sqrt{1 + i \frac{4 \tau^2 \mu \rho_o w}{\sigma^2 \Lambda^2 \varepsilon^2}} \right\} \quad (2.28)$$

Retaining this proposed model (Eq. 2.28) for the viscous dissipation effect, Allard and Champoux [81] proposed expressions for the dynamic bulk modulus for the same kind of porous material as a function of open porosity (ε), thermal characteristics length ($\bar{\lambda}$), static atmospheric pressure (P_o), specific heat ratio (γ), angular frequency (w) and thermal conductivity (k_T) of porous materials which was titled the Johnson–Champoux–Allard (JCA) model (Eq. 2.29).

$$K_{(w)} = \gamma \frac{P_o / \varepsilon}{\gamma - (\gamma - 1) \left\{ 1 - i \frac{8 k_T}{\bar{\lambda}^2 C_p \rho_o w} \sqrt{1 + i \frac{\bar{\lambda}^2 C_p \rho_o w}{16 k_T}} \right\}^{-1}} \quad (2.29)$$

The limitation for this model [73] was that the low-frequency limit of the real part of the dynamic mass density $\rho_{(w)}$ expression is not exact as ω tends to zero [73]. Similarly, the expression for $K_{(w)}$ was also not correct and the thermal characteristic length ($\bar{\lambda}$) was used to represent the medium at the high-frequency range of thermal effects. The expression of bulk modulus [79] (Eq. 2.29) was further modified by Lafarge et al. [24] with the introduction of a third non-acoustical microstructural parameter (static thermal permeability, (k'_0)) to describe the low-frequency behaviour of thermal effects termed the JCAL model (Eq. 2.30).

$$K_{(w)} = \gamma \frac{P_o / \varepsilon}{\gamma - (\gamma - 1) \left\{ 1 - i \frac{\varepsilon k_T}{k'_0 C_p \rho_o w} \sqrt{1 + i \frac{4 k'^2_0 C_p \rho_o w}{k \varepsilon^2}} \right\}^{-1}} \quad (2.30)$$

Despite the inclusion of static thermal permeability in the Johnson–Champoux–Allard model, the expression was still not deemed accurate, at low frequencies. Prides et al. [27] refined the JCA and JCAL expressions to describe the visco-inertial (five structural parameters) and thermal dissipative effects (four structural parameters) to obtain the complex density (Eq. 2.31) and bulk modulus (Eq. 2.32) of acoustic fluid for pores with motionless skeleton frame having arbitrary pore shapes. Also, theoretical determination of the static thermal permeability (k'_0), static viscous (τ_0) and static thermal (τ'_0) tortuosity were accounted

for by using dimensionless shape factors (M_1, M'_1, N_1 and N'_1) in Eq. (2.16) [47]. In summary, a total of eight structural parameters was needed to describe the propagation of a pressure wave through a porous structure backed by a rigid backing or back cavity using the JCAPL semi-phenomenological model.

where S_x in the proposed models is termed the Bessel function which is dependent on the pore geometry; D_p is the pore diameter size; P is the ambient pressure; γ is the specific heat ratio; ρ_o is the fluid density $w = 2\pi f$ is the angular frequency; μ is the fluid viscosity; C_p is the specific heat

$$\rho_{(w)} = \tau \frac{\rho_o}{\varepsilon} \left\{ 1 + \frac{\mu\varepsilon}{iw\rho_o k_o \tau} \left(1 - \frac{2k_o \tau}{\varepsilon \lambda^2 \left(\frac{\tau_o}{\tau} - 1\right)} + \frac{2k_o \tau}{\varepsilon \lambda^2 \left(\frac{\tau_o}{\tau} - 1\right)} \sqrt{1 + \frac{i\rho_o w \lambda^2 \left(\frac{\tau_o}{\tau} - 1\right)^2}{\mu}} \right) \right\} \quad (2.31)$$

$$K_{(w)} = \frac{\gamma P_o}{\varepsilon} \left[\gamma - (\gamma - 1) * \left[1 + \frac{k\varepsilon}{iw\rho_o C_p k'_o} * \left(1 - \frac{2k'_o}{\varepsilon \lambda'^2 (\tau'_o - 1)} + \frac{2k'_o}{\varepsilon \lambda'^2 (\tau'_o - 1)} \sqrt{1 + \frac{i\rho_o w C_p \lambda'^2 (\tau'_o - 1)^2}{k_\tau}} \right) \right] \right]^{-1} \quad (2.32)$$

1.4.3 Wilson Model

Due to the important role played by pore morphology and shape factor in the vibro-acoustical behavioural prediction of sound pressure waves across porous structures, Wilson [28] proposed a model to predict the complex density and bulk modulus of the structure with a triangular and circular aperture and near-spherical pore size. The model focused on the relaxation-matched behaviour of the porous medium and can predict the acoustical behaviour of porous materials regardless of its specific pore structure and the usual definition of low and high frequencies. Though more than one parameter (permeability, dynamic tortuosity, and porosity) is required to describe the acoustical behaviour of porous structures using Wilson’s model, it does provide a simpler representation with no Bessel and Kelvin functions [28] which is realistic at all frequencies. The simplified Wilson’s model for complex density (ρ_c) and bulk modulus ($K_{(w)}$) for circular and triangular pores are related to its complex specific volume (V_c) and complex compressibility ($\beta_{(w)}$) presented in Eqs. 2.33–2.35.

$$V_c = \frac{1}{\rho_c} = \frac{\varepsilon}{\rho_o \tau^2} + \left\{ 1 + \left(\frac{\tau^2}{\varepsilon} - 1 \right) S_x \left(D_p / \delta_{vor} \right) \right\} \quad (2.33)$$

$$\beta_{(w)} = \frac{1}{K_{(w)}} = \frac{\varepsilon}{P\gamma} \left\{ 1 + (\gamma - 1) S_x \left(D_p / \delta_{ent} \right) \right\} \quad (2.34)$$

$$S_x = \frac{3}{(1-i)x} \left\{ \coth(1-i)x - \frac{1}{(1-i)x} \right\}, \quad \delta_{vor} = \sqrt{\frac{2\mu}{w\rho_o}} \text{ and } \delta_{ent} = \sqrt{\frac{2k}{w\rho_o C_p}} \quad (2.35)$$

capacity at constant pressure; k is the thermal conductivity of the material; N_{pr} is the air Prandtl number; δ_{vor} and δ_{ent} are the vorticity and entropy mode boundary layer thickness respectively.

In order to accurately model the acoustic absorption of porous structures with near-spherical openings using Wilson’s model, it is necessary to specify the bulk modulus infinite frequency limit ($K_\infty = \frac{P\gamma}{\varepsilon}$), the density infinite frequency limit ($\rho_\infty = \frac{P\tau^2}{\varepsilon}$), the vorticity-mode relaxation time ($\tau_{vor} = \frac{2\rho_o \tau^2}{\varepsilon \sigma}$) and the entropy-mode relaxation time ($\tau_{ent} = N_{pr} \cdot \tau_{vor}$) in the physics modules acoustic software (typically, COMSOL Multiphysics 5.2™).

Other equivalent fluid models were developed to represent the surface acoustic impedance and normal incidence absorption coefficient of porous structures with specific pore morphologies. A typical example of this is the William EDFM model [82]. This model puts forward the expression of an effective density fluid model (EDFM) for acoustic propagation in sediment obtained from Biot’s theory with close agreement to their predicted values. Table 1 presents a tabular representation of the porous media acoustic model thereof, their applicability, limitations and structural parameters needed to fully describe the acoustic behaviour of porous materials.

Following the numerical simulation of pressure waves across sound absorbing materials [10, 11], the DBM model

Table 1 Acoustic porous media models

Models	Limitation	Application	Structural parameter(s)
Zwikker and Kosten [80]	All frequency	Straight cylindrical pores	ε , τ and k_o
Biot [79]	All frequency	Straight cylindrical pores	ε , τ and k_o
Attenborough [83]	All frequency	Sand and rigid fibrous	ε , τ , k_o , C_o and C_D
Delany and Bazley [78]	$0.01 < \frac{f}{\sigma} < 1.00$	Fibrous materials with straight cylindrical pores	k_o
Allard and Champoux [81]	$0.01 < \frac{f}{\sigma} < 1.00$	Fibrous materials with straight cylindrical pores	k_o
Miki [26]	$0.01 < \frac{f}{\sigma} < 1.00$	Fibrous materials with slanted cylindrical pores	k_o
Johnson et al. [59] and Allard and Champoux [81]	All frequency	Non-uniform section	ε , τ , k_o , Λ , and $\bar{\Lambda}$
Lafarge et al. [24]	Not exact low frequency	Non-uniform section	ε , τ , k_o , Λ , $\bar{\Lambda}$, and k'_0
Prides et al. [27]	All frequency	Non-uniform section with possible constrictions	ε , τ , k_o , Λ , $\bar{\Lambda}$, k'_0 , τ_0 and τ'_0
Wilson [28]	All frequency	Suitable for structures with circular and triangular pores	ε , τ , and k_o

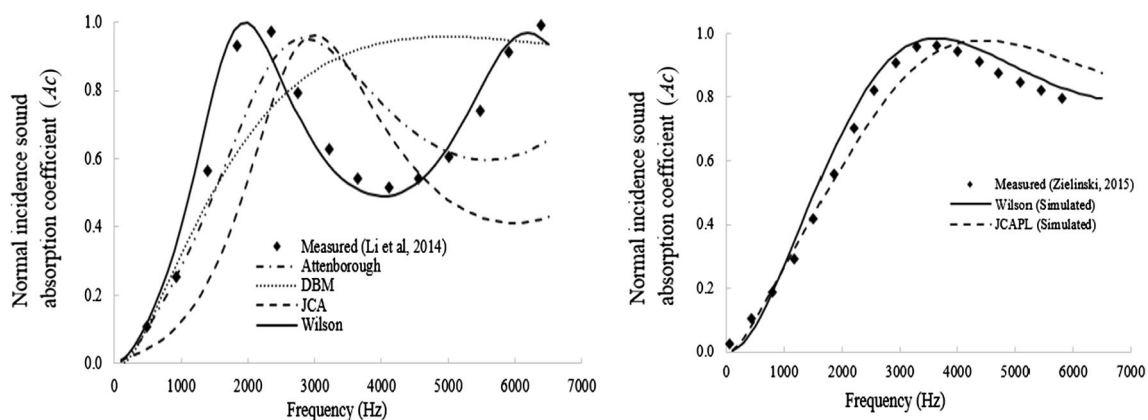


Fig. 12 Plots of measured and simulated normal incidence absorption coefficient for “bottleneck-type” porous aluminium structures of pore volume fraction 0.66 (left) and to the right is for porous ceramic foam

was reported to give an accurate prediction of the characteristic sound absorption spectra for glass wool fibre and melamine foam materials [3] which was attributable to their transversely isotropic nature, similar to that of fibrous materials. Interestingly, the DBM model was developed using experimental data on sound absorption spectra for fibrous materials. However, the DBM model fails to reliably predict the behaviour characterised by the dip in the sound absorption spectra for porous sintered fibre metals (observed to have a lower porosity than the fibrous materials [10, 11]). The JCA model shows a much better fit to the sound absorption spectra for this structure. Additionally, predictions using the JCA, JCAL, JCAPL and Attenborough models failed to reliably describe the measured characteristic absorption spectra for “bottleneck-type” structures over a large part of the frequency range [10, 11]. Figure 12 (left) shows that the Wilson equivalent fluid model for a rigid porous layer was evidently a good fit to the characteristic sound absorption spectra for both

structures characterised by pore volume fraction of 0.88. Adapted from Ref. [11]

“bottleneck-type” porous aluminium (0.66, pore volume fraction). Relatedly, a similar work [43] used the JCAPL semi-phenomenological model to estimate the surface acoustic impedance and normal incidence sound absorption coefficient for porous ceramic foam characterised by having a pore volume fraction of 0.88 (Fig. 12, right). Agreement between the measured and predicted sound absorption spectra using the JCAPL model was observably poor, especially for frequencies beyond 4 kHz when compared to the tolerable fit described in [11] using the Wilson equivalent fluid model.

1.5 Separating Low and High Frequencies Regime in a Porous Absorber

The pressure drop experiment in porous media described by the Henry Darcy law is often used for the determination of the static viscous permeability, as well as the airflow resistivity in porous materials [10, 11, 23, 25]. The description of the

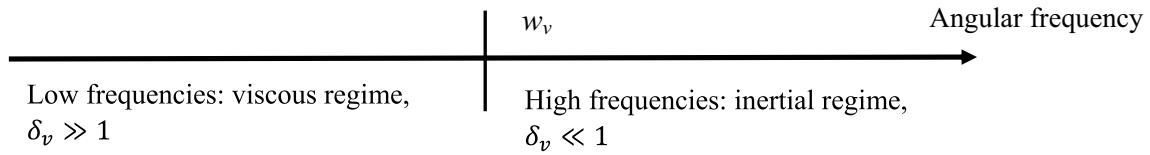
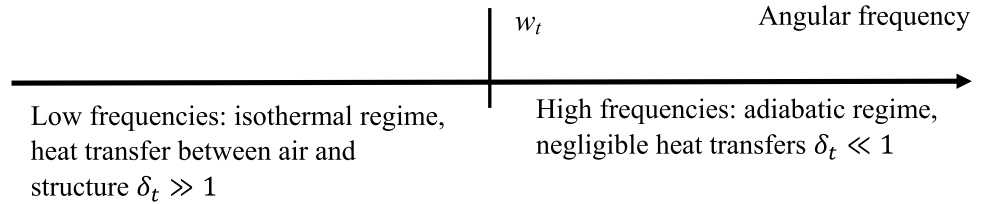


Fig. 13 Frequency-dependent visco-inertia dissipation mechanism

Fig. 14 Frequency-dependent thermal dissipation mechanism



acoustic properties of porous materials using the JCA semi-phenomenological five (5) parameters model accounts for the visco-inertial and thermal behaviour of acoustical materials. The resultant effect that arises from the creation of viscous and thermal boundary layers is because the separating (pore) fluid leaves the structural phase as pressure waves propagate through it. When viscous forces dominate inertial forces, it is termed the low-frequency regime and when inertial forces dominate viscous forces, it is termed the high-frequency regime [48]. A more realistic way of presenting this is in the use of a characteristic angular frequency presented in Figs. 13 and 14 below.

For the existence of a viscous boundary layer, when the pulsation is much smaller than the viscous characteristic angular frequency w_v and viscous boundary layer thickness much larger than unity ($\delta_v \gg 1$), the flow is purely viscous. Also, for pulsation much larger than the viscous characteristic angular frequency (w_v) and viscous boundary layer thickness much smaller than unity ($\delta_v \ll 1$), inertial effects dominate viscous effects. This is repeated for the classification of the thermal boundary layer in the low and high frequency regimes [59]. Below the thermal characteristic angular frequency (w_t), air compression and dilations are isothermal as heat transfer occurs between the fluid and structure [24]. Above the thermal characteristic angular frequency (w_t), it is classified as an adiabatic-regime with negligible heat transfer. This helps to distinguish between low and high-frequency regimes. Kirchhoff [85] derived mathematical relationships for the numerical determination of viscous and thermal boundary layer thickness as a function of fluid properties and frequency presented in Eqs. (2.36) and (2.37) below. The frequency is represented as f while δ_v , δ_t , η , ρ_o , k , C_p are the viscous boundary layer thickness, thermal boundary layer thickness, fluid dynamic viscosity, fluid density respectively, the thermal conductivity of the fluid and fluid specific heat capacity at constant pressure respectively.

Table 2 Estimation of viscous and thermal boundary layer thickness

$T = 20 \text{ }^\circ\text{C}$, $C_p = 1.0 * 10^3 \text{ (J/kg K)}$, $k = 2.6 * 10^{-2} \text{ (W/m K)}$, $\eta = 1.8 * 10^{-5} \text{ (N s/m}^2\text{)}$ and $\rho = 1.204 \text{ kg/m}^3$			
δ_v	$f = 100 \text{ Hz}$	$1.56 * 10^{-4} \text{ m}$	$\delta_v \ll 1 \sim$ high frequency inertial regime
	$f = 4500 \text{ Hz}$	$2.33 * 10^{-5} \text{ m}$	$\delta_v \ll 1 \sim$ high frequency inertial regime
δ_t	$f = 100 \text{ Hz}$	$1.85 * 10^{-4} \text{ m}$	$\delta_t \ll 1 \sim$ high frequency thermal regime
	$f = 4500 \text{ Hz}$	$2.77 * 10^{-5} \text{ m}$	$\delta_t \ll 1 \sim$ high frequency thermal regime

$$\delta_v = \sqrt{\frac{\mu}{\rho_o 2\pi f}} \tag{2.36}$$

$$\delta_t = \sqrt{\frac{k}{\rho_o C_p 2\pi f}} \tag{2.37}$$

The distinction between the viscous dominated (low frequency) regimes and inertial dominated (high-frequency) and that for the low and high frequency regimes for the thermal effects is shown (from a numerical computation) for a frequency range between 100 and 4500 Hz using Eqs. 2.36 and 2.37. Table 2 presents the calculated values of viscous and thermal boundary layer thickness for fluid properties obtained at standard atmospheric temperature and pressure. A simple analysis of visco-inertial and thermal dissipation effects for these audible frequency ranges show that for a porous metal to be a good sound absorber the pore openings (pore connectivity) should be in the order of 100 μm [5] or within the ranges of 10–1000 μm [47] and 11–350 μm [59]. Closed pore structures are characterised by very low openings [13] and an observable sound absorption coefficient from experimental

measurements of pressure wave across these structures in [5, 17] was considered poor. For “bottleneck-type” microcellular structures characterised by monomodal cells, the highest resonance peak in absorption was achieved [10, 11] for window-to-pore size ratio of 0.17 and permeability of $4.61 \times 10^{-10} \text{ m}^2$.

2 Conclusion

This review covers the acoustical properties and characterisation methods of sound-absorbing porous materials with an emphasis on “bottleneck-type” structures. The sound absorption spectra of different porous materials, pore-structure related parameters and acoustic porous media models available in the literature were also covered. From the available model, Wilson’s relaxation-matched equivalent fluid model was reported to be a good fit to the measured sound absorption spectra characterised by “bottleneck-type” materials. This enables an understanding of the changes associated with the pore-structure related parameters of the porous medium without the need for sample fabrication. The Wilson’s model was also reported to have used three pore-structure related parameters (porosity, permeability and dynamic tortuosity) to describe the relaxation behaviour at the scales of the pores and was developed for structures characterised by circular pores, a geometry that closely represents “bottleneck” structures. The sound absorption behaviour characterised by bimodal “bottleneck-type” structures is yet unknown although recent work has shown that the packing density of the bimodal structures could vary widely with pore volume fraction and other pore-structure related parameters. With the help of 3D advanced imaging techniques coupled with Multiphysics software, characterisation and modelling of the sound absorption spectra of bimodal structures may form an integral part of proposed future work.

Acknowledgements Dr. A.J. would like to acknowledge Prof. Andrew R. Kennedy (Lancaster University, Lancaster-UK), Prof. Herve P. Morvan (Technology Strategy Manager-CTO Office at Rolls-Royce, UK), Dr. Martin Corfield (The University of Nottingham-UK), The University of Nottingham Dean’s Award, Nottingham-UK, Petroleum Technology Development Fund, Abuja-Nigeria, Synopsis- Simpleware Ltd, California-USA and Bowers and Wilkins Group, West Sussex-UK for their financial and technical support.

References

1. FTCS (1969) *Fundamental of Telephone Communication Systems*. Western Electric Company. P2.1. en.wikipedia.org/wiki/sound06-01-2015
2. Y.X. Ou, *Flame Retardant-Manufacturing, Properties and Applications* (Weapon Industry Press, Beijing, 1997)
3. N. Kino, T. Ueno, Comparison between characteristic lengths and fiber equivalent diameter in glass fiber and melamine foam materials of similar flow resistivity. *J. App. Acoust.* **69**, 325 (2008)
4. X.Z. Deng, H.S. Liu, X.Y. Huang, Numerical simulation of effect of CO₂ content on cell nucleation in microcellular plastics extrusion processing for supercritical CO₂/PS. *Plast. Sci. Technol.* **36**(8), 30–32 (2008)
5. T.J.F. Lu, D. He, Sound absorption of cellular metals with semi-open cells. *J. Acoust. Soc. Am.* **108**(4), 1697–1708 (2000)
6. Y. Li, L. Zhendong, F. Han, Airflow resistance and sound absorption behaviour of open-celled aluminium foams with spherical cells. *Procedia Mater. Sci.* **4**, 187–190 (2014)
7. Z. Bo, C. Tianning, Calculation of sound characteristics of porous sintered fiber metal. *Appl. Acoust.* **70**, 337–346 (2009)
8. M.M. Muhammed, N.A. Sa’at, H. Naim, M.C. Isa, N.H.N. Yussof, M.S.D. Yati, *The Effect of Air Gap Thickness on Sound Absorption Coefficient of Polyurethane Foam* (Marine Material Research Group, Science and Technology Research, Institute of Defence, Ministry of Defence, Kuala Lumpur, 2013)
9. A.J. Otaru, H.P. Morvan, A.R. Kennedy, Modelling and optimisation of sound absorption in replicated microcellular metals. *Scr. Mater.* **150**, 152–155 (2018)
10. A.J. Otaru, Enhancing the sound absorption performance of porous metallic structures using tomography images. *Appl. Acoust.* **143**, 183–189 (2019)
11. A.J. Otaru, H.P. Morvan, A.R. Kennedy, Numerical modelling of the sound absorption spectra for bottleneck dominated porous metallic structures. *Appl. Acoust.* **151**, 164–171 (2019)
12. J. Zhou, Porous metallic materials, in *Advanced Structural Materials*, ed. by W.O. Soboyejo (CRC Press, Boca Raton, 2006), p. 22
13. H. Utsuno, T. Tanaka, T. Fujikawa, Transfer function method for measuring characteristic impedance and propagation constant of porous materials. *J. Acoust. Soc. Am.* **86**, 637–640 (1989)
14. Y.Y. Zhao, D.X. Sun, A novel sintering dissolution process for manufacturing Al foams powder metal. *Scr. Mater.* **44**, 105–110 (2001)
15. A.J. Otaru, *Review on processing and fluid transport in porous metals with a focus on bottleneck structures* (Mater. Int., Met, 2019). <https://doi.org/10.1007/s12540-019-00345-9>
16. A.J. Otaru, M.S. Muhammad, M.B. Samuel, A.G. Olugbenga, M.E. Gana, M.R. Corfield, Pressure drop in high-density porous metals via tomography datasets. *Met. Mater. Int.* (2019). <https://doi.org/10.1007/s12540-019-00431-y>
17. J.J. Lu, A. Hess, M.F. Ashby, Sound absorption of metallic foams. *Am. Inst. Phys.* **99**, 07511–07519 (1999)
18. A.R. Kennedy, *Porous Metals and Metal Foams made from Powders* (Manufacturing Division, University of Nottingham, Nottingham, 2012)
19. F. Han, G. Seiffert, Y. Zhao, B. Gibbs, Acoustic absorption Behaviour of an open-celled aluminium foam. *J. Phys. D* **36**, 294–302 (2003)
20. M. Lu, C. Hopkins, Y. Zhao, G. Seiffert, Sound absorption characteristics of porous steel manufactured by lost carbonate sintering. *Mater. Res. Soc. Symp. Proc.* **1188**, LL07-04 (2009)
21. J.T. Yeh, H.M. Yang, S.S. Huang, Combination of polyethylene filled with metallic hydroxides and cross-linkable polyethylene. *Polym. Degrad. Stab.* **50**(2), 229–234 (1995)
22. P.S. Liu, G.F. Chen, *Porous Materials Processing and Applications* (Tsinghua University Press Limited, Beijing, 2014), pp. 120–150
23. A.J. Otaru, Fluid flow and acoustic absorption in porous metallic structures using numerical simulation and experimentation. Ph.D. Thesis, The University of Nottingham, United Kingdom (2018)

24. D. Lafarge, P. Lemarinar, J.F. Allard, V. Tarnow, Dynamic compressibility of air in porous structures at audible frequencies. *J. Acoust. Soc. Am.* **102**(4), 1–12 (1997)
25. A.J. Otaru, A.R. Kennedy, The permeability of virtual macroporous structures generated by sphere-packing models: comparison with analytical models. *Scr. Mater.* **124**, 30–33 (2016)
26. Y. Miki, Acoustical properties of porous materials-modifications of Delany Bazley model. *J. Acoust. Soc. Jpn (E)* **11**(1), 19–24 (1990)
27. S.R. Prides, F.D. Morgan, A.F. Gangi, Drag forces of porous-medium acoustics. *Phys. Rev. B* **47**, 4964–4978 (1993)
28. K. Wilson, Relaxation-matched modelling of propagation through porous media, including fractal pore structure. *J. Acoust. Soc. Am.* **94**(2), 1136–1145 (1993)
29. M.F. Ashby, A. Evans, A.R. Kennedy, The role of oxidation during compaction on the expansion and stability of Al foams made via a PM route. *Adv. Eng. Mater.* **8**, 568–570 (2006)
30. P. Langston, A.R. Kennedy, Discrete element modelling of the packing of spheres and its application to the structure of porous metals made by infiltration of packed beds of NaCl beads. *Powder Technol.* **268**, 210–218 (2014)
31. A.J. Otaru, H.P. Morvan, A.R. Kennedy, Measurement and simulation of pressure drop across replicated microcellular aluminium in the Darcy–Forchheimer regime. *Acta Mater.* **149**, 265–275 (2018)
32. A.J. Otaru, H.P. Morvan, A.R. Kennedy, Airflow measurement across negatively infiltration processed porous aluminium structures. *AIChE J.* (2019). <https://doi.org/10.1002/aic.16523>
33. A.J. Otaru, A.R. Kennedy, Investigation of the pressure drop across packed beds of spherical beads: comparison of empirical models with pore-level computational fluid dynamics simulations. *ASME Fluids Eng.* (2019). <https://doi.org/10.1115/1.4042957>
34. F. Sun, H. Chen, J. Wu, K. Feng, Sound absorbing characteristics of fibrous metal materials at high temperature. *Appl. Acoust.* **71**, 221–235 (2010)
35. K. Attenborough, Models for the acoustical characteristics of air-filled granular materials. *Acta Acoust.* **1**, 213–226 (1993)
36. O. Umnova, K. Attenborough, E. Stanley, A. Cummings, Behaviour of rigid-porous layers at high levels of continuous acoustic excitation: theory and experiment. *J. Acoust. Soc. Am.* **114**, 1346–1356 (2003)
37. M.C.M. Wright, *Lecture Notes on the Mathematics of Acoustics* (University of Southampton, Imperial College Press (ICP), London, 2005), pp. 157–161
38. D.A. Bies, C.H. Hansen, *Engineering Noise Control* (Spon Press, New York, 2009)
39. C. Lautensack, M. Kabel, *Modelling and Simulation of Acoustic Absorption of Open Cell Metal Foams, Cellular Metals for Structural and Fundamental Applications* (Fraunhofer IFAM, Dresden, 2009), pp. 271–276
40. Q.Z. Wang, D.M. Lu, C.X. Cui, L.M. Liang, Material science and engineering. *J. Mater. Process. Technol.* **211**, 363 (2011)
41. J.M. Qiam, X.X. Li, Preparation of newly sound-absorbing PVC matrix foam. *Plast. Sci. Technol.* **47**(4), 5–8 (2000)
42. Y. Champoux, M.R. Stinson, On acoustical models for sound propagation in rigid frame porous materials and the influence of shape factors. *J. Acoust. Soc. Am.* **92**(2), 1120–1131 (1992)
43. Y. Li, X. Wang, X. Wang, Y. Ren, F. Han, C. Wen, Sound absorption characteristics of aluminium foam with spherical cells. *J. Appl. Phys.* **110**, 113525 (2011)
44. T.G. Zielinski, Generation of random microstructures and prediction of sound velocity and absorption for open foams with spherical pores. *J. Acoust. Soc. Am.* **137**(4), 1790–1801 (2015)
45. M.P. Norton, D.G. Karszub, *Fundamental of Noise and Vibration Analysis for Engineers* (Cambridge University Press, Cambridge, 2003)
46. M.J. Crocker, *Handbook of Noise and Vibration Control* (Wiley, Hoboken, 2007)
47. C. Perrot, F. Chevillotte, L. Jaouen, M.T. Hoang, *Acoustic Properties and Applications* (DESTTECH Publication, Inc. Technology & Engineering, Lancaster, 2013)
48. N. Dukhan, *Metal Foams: Fundamental and Applications* (DESTTECH Publication, Inc. Technology & Engineering, Lancaster, 2013), pp. 1–310
49. B. Hinze, J. Rosler, Measuring & simulating acoustic absorption of open-celled metals. *Adv. Eng. Mater.* **16**(3), 284–288 (2014)
50. H. Oun, A.R. Kennedy, Tailoring the pressure drop in multi-layered open-cell porous inconel structures. *J. Porous Mater.* **2**, 1627–1633 (2015)
51. L.L. Beranek, Acoustic impedance of porous materials. *J. Acoust. Soc. Am.* **13**, 248–260 (1942)
52. F.A.L. Dullien, *Porous Media: Fluid Transport and Pore Structure*, 2nd edn. (Academic Press, London, 2012), pp. 6–110
53. H. Oun, A.R. Kennedy, Experimental investigation of pressure drop characterization across multilayer porous metal structure. *J. Porous Mater.* **21**, 1133–1141 (2014)
54. A.B. Abell, K.L. Willis, D.A. Lange, Mercury intrusion porosimetry and image analysis of cement-based materials. *J. Colloid Interface Sci.* **211**, 39–44 (1999)
55. J. Petrasch, P. Wyss, A. Steinfeld, Tomography-based monte carlo determination of radiative properties of reticulated porous ceramics. *J. Quant. Spectrosc. Radiat. Transf.* **105**, 180–197 (2007)
56. K.K. Bodla, J.Y. Murthy, S.V. Garimella, *Microtomography-Based Simulation of Transport through Open-Cell Metal Foams* (CTRC Research Publication, Purdue University e-Pubs, West Lafayette, 2010), pp. 527–544
57. S. Peng, Q. Hu, S. Dultz, M. Zhang, Using X-ray computed tomography pore structure characterization for berea sandstone: resolution effect. *J. Hydrol.* **472–473**, 254–261 (2012)
58. T.P. De Carvalho, H.P. Morvan, D. Hargreaves, H. Oun, A. Kennedy, Pore-scale numerical investigation of pressure drop behaviour across open-cell metal foams. *Transp. Porous Media* **117**(2), 311–336 (2017)
59. D.L. Johnson, J. Koplik, R. Dashen, Theory of dynamic permeability & tortuosity in fluid-saturated porous media. *J. Fluid Mech.* **176**, 176–402 (1987)
60. P.M. Adler, *Porous Media: Geometry and Transport* (Butterworth-Heinemann, Boston, 1992)
61. G.E. Archie, The electrical resistivity log as an aid in retaining some reservoir characteristics. *Trans. AIME* **116**, 54–62 (1942)
62. W.O. Winsaur, H.M. Shearin Jr., P.H. Masson, Resistivity of brine-saturated sand in related to pore geometry. *Am. Assoc. Pet. Geol. Bull.* **36**, 203–211 (1952)
63. C.N. Satterfield, *Mass Transfer in Heterogeneous Catalysis* (MIT Press, Cambridge, 1970)
64. T.G. Zielinski, Inverse identification and microscopic estimation of parameters for models of sound absorption in porous ceramics, in *Proceeding of International Conference on Noise and Vibration Engineering, International Conference on Uncertainty in Structural Dynamics* (2013), pp. 95–109
65. H.L. Weissberg, Effective diffusion coefficient in porous media. *J. Appl. Phys.* **34**, 2636 (1963)
66. M. Matyka, A. Khalili, Z. Koza, Tortuosity-porosity relation in porous media flow. *Phys. Rev. E* **78**, 026306 (2008)
67. A. Bhattacharya, V.V. Calmidi, R.L. Mahajan, Thermo-physical properties of high porosity metal foams. *Int. J. Heat Mass Transf.* **45**, 1017 (2002)

68. P. Du Plessis, A. Montillet, J. Comiti, Pressure-drop prediction for flow through high porosity metallic foams. *Chem. Eng. Sci.* **49**, 3545–3553 (1994)
69. J.P. Du Plessis, J.G. Fourie, Pressure drop modelling in cellular metallic foams. *Chem. Eng. Sci.* **57**, 2781–2789 (2002)
70. R. Dias, J.A. Teixeira, M. Mota, A. Yelshin, Tortuosity variation in a low-density binary particulate beds. *Sep. Purif. Technol.* **51**(2), 180–184 (2006)
71. P. Guo, Lower and upper bounds for hydraulic tortuosity of porous materials. *Transp. Porous Media* **109**, 659–671 (2015)
72. X. Olny, R. Panneton, J. Van Tran, *Experimental Determination of Acoustical Parameters of Rigid and Limp Materials Using Direct Measurements and Analytical Solutions* (G.A.U.S Department of Mechanical Engineering, Universite de Sherbrooke, Sherbrooke, 2003), pp. 1–6
73. X. Olny, R. Panneton, Acoustic determination of the parameters governing thermal dissipation in porous media. *J. Acoust. Soc. Am.* **123**, 814–824 (2008)
74. D.L. Johnson, T.J. Plana, C. Scala, F. Pasierb, H. Kojima, Tortuosity & acoustic slow waves. *Phys. Rev. Lett.* **49**, 1840–1844 (1982)
75. P. Leclaire, L. Kelder, M. Lauriks, M. Melon, N. Brown, B. Cata-gende, *Determination of the viscous and thermal characteristic length of plastic foam by ultrasonic measurement in helium and air* (*J. Appl., Phy.*, 2012), p. 80
76. B.H. Song, J.S. Bolton, A transfer-matrix approach for estimating the characteristic impedance and wave number of limp and rigid porous materials. *J. Acoust. Soc. Am.* **107**(3), 1131–1152 (2000)
77. W.T. Chu, Impedance tube measurements: a comparative study of current practices, in *Proceedings of the International Conference on Noise Control Engineering: Engineering for Environmental Noise Control: Inter-Noise '89, Newport Beach, CA, USA* (1989)
78. M.E. Delany, E.N. Bazley, Acoustical properties of fibrous absorbent materials. *Appl. Acoust.* **3**(2), 105–116 (1970)
79. M.A. Biot, Theory of propagation of elastic waves in a fluid-saturated porous solid II: higher frequencies range. *J. Acoust. Soc. Am.* **28**(2), 168–178 (1956)
80. C. Zwikker, C.W. Kosten, *Sound Absorbing Materials* (Elsevier, New York, 1949)
81. J.F. Allard, Y. Champoux, New empirical equations for sound propagation in rigid frame fibrous materials. *J. Acoust. Soc. Am.* **91**(6), 3346–3353 (1992)
82. K.L. William, An effective density fluid model for acoustic propagation in sediments derived from Biot's theory. *J. Acoust. Soc. Am.* **110**, 2276–2281 (2001)
83. K. Attenborough, Acoustical characteristics of rigid fibrous absorbents & granular materials. *J. Acoust. Soc. Am.* **73**, 785–799 (1983)
84. P.W. Jones, *Measuring and Simulation of Acoustic Performance of Polyurethane Foam Filled Muffler: A Case Study* (University of New South Wales, Sydney, 2010)
85. G. Kirchoff, in *On the Influence of Heat Conduction in a Gas on Sound Propagation*, ed. by R.B. Lindsay (Dowden, Hutchinson & Ross, Stroudsburg, 1974)

Publisher's Note Springer Nature remains neutral with regard to jurisdictional claims in published maps and institutional affiliations.